Accepted Article

This manuscript has been accepted after peer review and appears as an Accepted Article online prior to editing, proofing, and formal publication of the final Version of Record (VoR). This work is currently citable by using the Digital Object Identifier (DOI) given below. The VoR will be published online in Early View as soon as possible and may be different to this Accepted Article as a result of editing. Readers should obtain the VoR from the journal website shown below when it is published to ensure accuracy of information. The authors are responsible for the content of this Accepted Article.

WILEY-VCH

COMMUNICATION

Titanium-Phosphonate-Based Metal-Organic Frameworks with Hierarchical Porosity for Enhanced Photocatalytic Hydrogen Evolution

Hui Li,[a] Ying Sun,[a] Zhong-Yong Yuan,[b] Yun-Pei Zhu,*[c] and Tian-Yi Ma*[d]

Photocatalytic hydrogen production is crucial for solar-to-chemical conversion process, wherein high-efficiency photocatalysts lie in the heart of this area. Herein a new photocatalyst of hierarchically mesoporous titanium-phosphonate-based metal-organic frameworks, featuring well-structured spheres, periodic mesostructure and large secondary mesoporosity, are rationally designed with the complex of polyelectrolyte and cathodic surfactant serving as the template. The well-structured hierarchical porosity and homogeneously incorporated phosphonate groups can favor the mass transfer and strong optical absorption during the photocatalytic reactions. Correspondingly, the titanium phosphonates exhibit significantly improved photocatalytic hydrogen evolution rate along with impressive stability. This work can provide more insights into designing advanced photocatalysts for energy conversion and render a tunable platform in photoelectrochemical field.

Producing renewable hydrogen energy from water splitting represents a prospective means of storing solar energy in a way of compensating for the intermittency of sunlight as a central source of power.[1,2] To date, various inorganic and organic semiconductor photocatalysts have been developed in an attempt to harvest and convert sunlight to achieve water photolysis,[3,4] though the further improvement of the proof-of-principle systems is impeded by the insufficient absorbance and unfavorable spatial separation efficiency of photoinduced charge carriers, while the key is to develop new materials with novel structures. One one side, atomic modulation (*e.g.*, element doping) is an efficient way to extend light absorption range and reduce charge transfer barrier through modifying the semiconductors' electronic structures,[5,6] but high-temperature and tedious stepwise processes are required. On the other side, introducing porosity and/or micro-/nanostructures can ensure the accessibility of active sites in the fine pore systems, shorten the photocarrier transportation distance, and promote the mass transfer, thus leading to improved reaction kinetics.[7,8] Noticeably, rational assembly of different surfactants, such as polyelectrolytes and oppositely charged surfactants, can favor the formation of dynamic templates to afford interesting nanostrucutes with novel porosity,[9,10] for instance, hierarchically porous nanoplates and nanorods. As fascinating functional templates, the organic matrices from the cooperative organization of different templating agents are promising in synthetizing efficient photocatalysts. However, how to synthesize advanced photocatalysts with the superiorities of atomic modification and new pore/structure systems through a surfactant-directed strategy remains urgent and challenging.

Different from inorganic or organic materials, metal-organic frameworks (MOFs) are constructed by inorganic metal centers/clusters and organic linkers intimately and periodically, while the organic components can make MOFs versatile for exploiting intelligent materials which can manifest a response due to external stimuli.[11,12] Through adjusting either the metallic or organic constituents, not only the surface functionality but also the light absorbance of MOFs can be readily tuned.[13,14] Carboxylate-based MOFs have been investigated for photocatalytic hydrogen evolution, whereas precious photosensitizers/photoactive linkers and additional cocatalysts need to be integrated into the systems for enabling light-driven proton reduction; moreover, the poor coordination ability of carboxylate ligands and insufficient porosity (pore size generally smaller than 2 nm) pose major challenges in operation stability and apparent activity enhancement.[15,16] Distinctively, metal-phosphonate-based MOFs with controllable porosity, such as titanium phosphonates, feature remarkable stability due to the robust R–P–O–metal bonds (R: organic functional groups).[17,18] Furthermore, the introduction of phosphonic functional linkers can shift the absorption edge of titanium phosphonates to visible region relative to pristine titania, owing to the homogeneous incorporation of phosphorus and carbon species.[19] In spite of widespread applications of metal phosphonates in energy-related areas like proton conductors and organic contaminant photodegradation,[17-19] metal phosphonates have thus far been understudied towards photocatalytic hydrogen production.

Herein hierarchically mesoporous titanium phosphonates (denoted as HM-TiPPh) are prepared via a facile hydrothermal]¦[&^••Á¸âc@Ác@^Á˘•^Á[~Á][|^^|^&c¦[|^c^ •˘¦-æ&cæ}cÁ&[{]|^¢^•Áæ•Á the template. The resultant well-defined mesoporosity and homogeneous integration of organic moieties impart enhanced capabilities of mass transfer and light absorption, ensuring the application of the hierarchically mesoporous titanium phosphonates in photocatalytic hydrogen evolution with considerable performance.

The preparation of HM-TiPPh involved the condensation between $TiCl_4$ and 1-hydroxyethylidene-1,1-diphosphonic acid

[a] Dr. H. Li, Dr. Y. Sun
Liaoning Key Laboratory for Green Synthesis and Preparative Chemistry of Advanced Materials
College of Chemistry, Liaoning University
Shenyang 110036, China
[b] Prof. Z. Y. Yuan
School of Materials Science and Engineering
Nankai University
Tianjin 300353, China
[c] Dr. Y. P. Zhu
Materials Science and Engineering
King Abdullah University of Science and Technology (KAUST)
Thuwal 23955-6900, Saudi Arabia
E-mail: yunpei.zhu@kaust.edu.sa
[d] Dr. T. Y. Ma
Discipline of Chemistry, School of Environmental and Life Sciences
University of Newcastle
Callaghan, NSW 2308, Australia
E-mail: tianyi.ma@newcastle.edu.au

Supporting information for this article is given via a link at the end of the document.

COMMUNICATION

(HEDP) in the presence of cationic surfactant cetyltrimethylammonium bromide (CTAB) and anionic polymer poly(acrylic acid) (PAA) through a hydrothermal process, wherein the complex colloids co-assembled by CTAB and PAA via electrostatic interaction served as structure-directing agents to form hierarchical mesoporosity. Low-resolution scanning electron microscopy (SEM) image reveals high-yield spheres of HM-TiPPh, of which the average diameter is 400–600 nm (Figure 1a). Rough surface of a single sphere can be observed at a higher resolution (Figure 1b). Low-resolution transmission electron microscopy (TEM) image exhibits different contrast inside the spheres (Figure 1c), suggesting the existence of interstitial pores. A further magnification shows the periodic mesostructure with pore size of approximately 3 nm within the whole spherical nanoparticle together with secondary mesopores with larger size (Figure 1d). Moreover, the homogeneous dispersion of Ti and P elements throughout the spheres confirms the compositional homogeneity within the network, as evidenced by energy dispersive X-ray spectroscopy (EDS) elemental mapping images (Figure S1).

mesophase symmetry. This implies that HM-TiPPh possesses intraparticle mesoporosity with long-range order, consistent with the TEM observation. The wide-angle XRD pattern reflects the amorphous nature of HM-TiPPh without detectable TiO_2 phase (Figure 1e, inset), indicating the extensive condensation of organophosphonic linkers and metallic precursors to form an extensive metal-organic framework. Additionally, HM-TiPPh shows the N_2 sorption isotherm of type IV with two obvious hysteresis loops respectively in the relative pressure range of 0.25–0.5 and 0.75–0.96 (Figure 1f). The first adsorption step relates to one narrow peak at 3.1 nm in the pore size distribution curve, indicative of ordered mesopores with uniform pore size, while the second step affords a broad pore size centered at about 30 nm, assignable to the secondary interstitial mesopores. The third adsorption at high relative pressure can be attributable to voids from the aggregation of spheres and possibly large nanopores inside the spheres. Accordingly, HM-TiPPh possesses a high surface area and a large pore volume of 448 m^2 g^{-1} and 1.06 cm^3 g^{-1}, respectively, signifying its superior textual properties.

Figure 2. Schematic illustration of the formation process of hierarchically porous titanium phosphonates using dual templates.

The formation mechanism of the delicate mesostructure is based on the ionic self-assembly of surfactant and oppositely charged polyelectrolyte that can create ordered mesomorphous liquid crystalline phases.[20,21] Firstly, the co-organization of cationic cetyltrimethylammonium (CTA) micelles and anionic PAA leads to the formation of highly ordered mesophases and mesomorphous PAA-CTA complexes through electrostatic interaction (Figure 2),[22] wherein the negatively charged phosphonic molecules can also be homogeneously incorporated into the supramolecular complexes. Upon adding active $TiCl_4$ species, the hydrolysis and polymerization between $TiCl_4$ and phosphonic groups to give electronegative titanium phosphonate oligomers can disarrange the electrostatic interaction between CTA and PAA, inducing the reassembly of the mesophase. Titanium phosphonate species can interact with the ordered mesomorphous complexes and cross-link around the cationic micelles to afford ordered mesostructure. Moreover, the interactions between negatively charged PAA supramolecules and positively charged CTA micelles are disturbed, resulting in the disassociation of some PAA chains from the mesomorphous complexes to render phase-separated PAA chain domains, which act as the templates for the formation of interstitial pores inside the spheres.[23] For comparison, mesoporous titanium

Figure 1. (a, b) SEM, (c, d) TEM images of HM-TiPPh. (e) Low-angle and (inset of e) wide-angle XRD pattern of HM-TiPPh. (f) N_2 adsorption-desorption isotherm and (inset of f) the corresponding pore size distribution curve.

The small-angle XRD pattern of HM-TiPPh, conducted to investigate its mesostructure, presents a series of diffractions, which can be indexed to (111), (200), (220), and (311) diffractions (Figure 1e), respectively, characteristics of cubic *Fm-3m*

COMMUNICATION

phosphonate materials (marked as M-TiPPh, Figure S2 and S3) without porous hierarchy were synthesized without cationic polyelectrolyte, corroborating the critical role of PAA in forming hierarchical porosity.

Figure 3. (a) ^{31}P and (b) ^{13}C MAS NMR spectra of HM-TiPPh. High-resolution XPS spectra of the Ti 2p (c) and P 2p (d) core levels in HM-TiPPh.

HM-TiPPh's skeleton characteristics were confirmed by Fourier transform infrared (FT-IR) spectra, magic angle spinning nuclear magnetic resonance (MAS NMR), and X-ray photoelectron spectroscopy (XPS). In the FT-IR spectra (Figure S4), the sharp band situated at 1065 cm^{-1} is related to P–O–Ti stretching vibrations, while the typical P–OH stretching vibration at around 930 cm^{-1} cannot be detected,[24] both of which reveal the formation of extensive titanium phosphonate network. The ^{31}P MAS NMR spectra of HM-TiPPh shows one symmetric peak at 12.1 ppm (Figure 3a) together with the broadening of the resonance signal, characteristic of amorphous metal phosphonates.[18,25] In the ^{13}C MAS NMR spectra (Figure 3b), two signals at 20.7 and 72.3 ppm can be ascribed to the carbon atom in the terminal methyl group and the quaternary carbon atom connected with the P=O group, respectively.[26]

The XPS survey spectrum illustrates that HM-TiPPh contains four types of elements including Ti, P, O, and C, without other detectable impurities (Figure S5). The surface P/Ti atomic ratio is determined to be 1.36, close to 4:3 for the P/Ti feeding ratio. The Ti 2p core level (Figure 3c) manifests two signal peaks at 458.2 eV (Ti 2p$_{3/2}$) and 464.2 eV (Ti 2p$_{1/2}$), corresponding to the Ti species in P–O–Ti.[18] Noticeably, the binding energy of the main Ti 2p for HM-TiPPh decreases in comparison with that of pristine TiO$_2$ (458.8 eV for Ti 2p$_{3/2}$ and 464.6 eV for Ti 2p$_{1/2}$, Figure S6),[27] caused by the strong interaction between phosphonic linkers and Ti centers. A symmetrical peak at 131.2 eV in P 2p XPS spectrum is characteristic of P^{5+} in the phosphonate groups (Figure 3d).[28] The deconvolution of O 2s line delivers a main signal at 529.4 eV and a shoulder around 531.5 eV can be

ascribed to bridging oxygen in the P–O–Ti linkages and surface hydroxyl, respectively (Figure S5).[18,28] Besides, the P/Ti molar ratio of 4:3 determined by inductively coupled plasma (ICP) emission spectroscopy, together with the thermal gravimetric (TG) (Figure S7) analysis, EDS, FT-IR, XPS, and NMR, suggest no phase separation during the synthesis and organophosphonic moieties can act as efficient linkers to connect transition metals to form an extensive metal-organic network.

Figure 4. (a) UV-vis diffuse reflectance spectra of TiO$_2$ and HM-TiPPh (Inset: the corresponding Tauc plots). Typical time course of hydrogen evolution catalyzed by the synthesized photocatalysts under the irradiation of visible light (b) and simulated sunlight (c). (d) Long-term durability tests of HM-TiPPh under visible light illumination. (e) Photocurrent response curves and (f) PL emission spectrum of HM-TiPPh, M-TiPPh, and TiO$_2$.

Indeed, the introduction of phosphonic group results in bathochromic shift of photoabsorption edge and an increase of light harvesting across the wavelength region investigated in comparison with TiO$_2$, as illustrated by ultraviolet–visible diffuse reflectance spectroscopy (Figure 4a). This improved light absorbance is also believed to reflect the capability of the hierarchical mesoporosity to provide multiple scattering within the spheres, promoting the efficient path length for light harvesting.[29,30] Different from the band-to-band photoabsorption for TiO$_2$, an apparent absorption tail (known as Urbach tail) for HM-TiPPh can be related to the electronic states situated within the band gap (midgap states),[31,32] considerably contributing to capturing the photons with energy even smaller than the band gap,

COMMUNICATION

which accordingly leads to the appearance of a Urbach photoabsorption tail. This phenomenon is similar to chemically doped semiconductor photocatalysts,[33,34] suggesting the positive role of homogeneous doping of carbon and phosphorus introduced by the organic coupling molecules in improving photoenergy absorption.[19,28] The optical band gap (E_g) value of HM-TiPPh is determined to be 2.73 eV according to the Tauc curve (Figure 4a, inset, see calculation in Supporting Information), lower than that of TiO_2 (3.03 eV). Additionally, the Tauc plot of HM-TiPPh manifests an apparent tail between 2.0 and 2.8 eV, which is beneficial to enhance the light absorption and the photocatalytic efficiency.[30]

The well-structured porosity and homogeneous incorporation of organic motifs can favor the fast mass transport and enhance light energy harvest, thereby creating a promising platform in photocatalytic water splitting to produce hydrogen. Under the visible light irradiation ($\lambda > 400$ nm, Figure 4b), a remarkable H_2 production rate of 945 µmol h^{-1} g^{-1} is achieved on HM-TiPPh, outperforming that of TiO_2 (249 µmol h^{-1} g^{-1}). In contrast, M-TiPPh exhibits a lower mass-specific activity (698 µmol h^{-1} g^{-1}) than HM-TiPPh, revealing the significant role of large secondary nanopores in boosting the performance. Impressively, the considerable visible-light-driven hydrogen evolution activity of HM-TiPPh is comparable or even superior to most of the state-of-the-art TiO_2-based photocatalysts and other catalytic systems, for instance, sub-10 nm rutile TiO_2 nanoparticles (932 µmol h^{-1} g^{-1}),[35] CuO_x/TiO_2 (670 µmol h^{-1} g^{-1}),[36] and UiO-66-NH$_2$ with Pt nanoparticles introduced[16] (see detailed comparison in Table S1). After exposure to full-spectrum simulator illumination (Figure 4c), HM-TiPPh presents a hydrogen evolution rate of 1873 µmol h^{-1} g^{-1}, 1.58 and 3.21 times larger than that of M-TiPPh (1185 µmol h^{-1} g^{-1}) and TiO_2 (584 µmol h^{-1} g^{-1}), respectively, coinciding with the trend observed under visible light irradiation.

Stability is another crucial parameter to evaluate a practical catalyst. No significant attenuation of hydrogen evolution rate for HM-TiPPh can be observed after four consecutive operations under a prolonged visible light irradiation of 16 h (Figure 4d). HM-TiPPh still maintains most of the inherent catalytic reactivity without significant inactivation even after storage in the reaction solutions for two weeks (Figure S8). Note that there is no obvious alternation of the intrinsic structure and textual property of HM-TiPPh before and after multiple photocatalytic reactions (Figure S9), verifying the robust nature of the titanium phosphonates against photocorrosion.

The efficient diffusion process plays an important role in expediting photocatalytic reactions, as verified by electrochemical impedance spectroscopy (EIS). In the EIS Nyquist plots (Figure S10), the Warburg-type line of HM-TiPPh at low frequency range assigned to electrolyte diffusion and transport within catalysts is shorter than that of M-TiPPh, implying the fast electrolyte diffusion and transfer through the hierarchically porous structures.[37] By normalizing the hydrogen evolution rate by the specific surface area, the value of M-TiPPh (2.17 µmol h^{-1} g^{-1} m^{-2}) is slightly higher than that of HM-TiPPh (2.11 µmol h^{-1} g^{-1} m^{-2}), though HM-TiPPh possesses a larger surface area than that of M-TiPPh, suggesting that the photocatalytic activity is not simply proportional to the surface area but also closely associated with the pore structure. As such, the higher activity of HM-TiPPh than the mesoporous counterpart can be preferably related to the elevated mass transfer of reactants and products within the well-structured hierarchical pores that can efficiently promote the reaction kinetics.

According to the transient photocurrent response curves (Figure 4e), all the photocatalysts exhibit rapid and entirely reversible photocurrent response upon each light excitation. Notably, the photocurrent density of HM-TiPPh is obviously higher than that of M-TiPPh and TiO_2, revealing its enhanced separation and mobility of the photoexcited charge carriers. Photoluminescence (PL) originates from the recombination of free charge carriers, making it feasible to evaluate the separation/recombination efficiency of photoinduced charge carriers qualitatively.[38] Evidently, the remarkable PL quenching of HM-TiPPh in principle illustrates the largely suppressed energy-wasteful recombination of charge carriers (Figure 4f), thereby boosting photocatalytic activities greatly. The polarization curves display increasing currents with the decrease of cathodic potential (Figure S11), corresponding to the water reduction to evolve hydrogen. The low overpotential and pronounced current density for HM-TiPPh indicate the favorable reaction kinetics and enhanced photocatalytic activity. On one hand, the increased light absorbance for titanium phosphonates than that of TiO_2 can contribute to the enhanced photocurrents due to the metal-organic framework with homogeneous carbon and phosphorus doping; one the other hand, the structural superiority can improve the separation efficiency of the photoinduced charge carriers and their transfer rates, since the well-defined spheres and hierarchical nanopores can shorten the diffusion length of charge transfer and promote the electron relocalization on surface terminal sites to prohibit the charge recombination.[39,40]

The (photo)electrochemical results demonstrate the same trend to the photocatalytic activity testing, unambiguously revealing the advantages of well-structured hierarchical porosity for high-performance photocatalysis. After mechanical ball-milling to destroy the structural/textual characteristics, the resultant titanium phosphonate manifests largely decreased activity as a result of losing porosity, nanostructure and increased charge transfer resistance (Figure S10, S12, S13), further confirming the structural peculiarity in boosting photoactivity. Generally, heterogeneous photocatalytic water splitting process undergoes three consecutive processes: light harvest, photocarrier generation/separation/migration and surface redox reactions, which are intimately related to the electronic, surface, compositional and structural properties of the photocatalytic systems. Herein the homogeneous doping of carbon and phosphorus originated from the phosphonic linkages endows the MOF framework with narrowed band gap and extended light absorption, ensuring the better use of optical energy. Further, the favorable structural/textual characteristics (spheres and hierarchical porosity) can not only enhance the charge mobility but also contract the diffusion distance from internal towards the surface. Also, the hierarchical nanopores are capable of providing abundant active centers and open spaces to allow the electrolytes to easily penetrate and to ensure the fast release of products to instantly expose active sites. Consequently, a synergistic improvement in the photocatalytic performance through the aforementioned aspects is realized.

To conclude, hierarchically mesoporous titanium phosphonates prepared through a coupled-template method

COMMUNICATION

possessed high surface areas, ordered mesostructure, and large secondary nanopores, affording smooth pathway for fast transportation of electrolytes and products. The textual and structural features along with favorable behavior of light harvest ensured the superb photocatalytic hydrogen evolution performance. The results presented here afford new methodologies in designing novel photocatalysts with considerable activity. A further step can be expected to synthesize hierarchically porous materials with various mesostructures through tuning the combination of oppositely charged surfactants to realize advanced catalyst systems.

Acknowledgements

1. Y. Kofuji, Y. Isobe, Y. Shiraishi, H. Sakamoto, S. Tanaka, S. Ichikawa, T. Hirai, *J. Am. Chem. Soc.* **2016**, *138*, 10019–10025.
2. K. S. Lakhi, D. H. Park, K. Al-Bahily, W. Cha, B. Viswanathan, J. H. Choy, A. Vinu, *Chem. Soc. Rev.* **2017**, 46, 72–101.
3. Y. Ide, N. Inami, H. Hattori, K. Saito, M. Sohmiya, N. Tsunoji, K. Komaguchi, T. Sano, Y. Bando, D. Golberg, Y. Sugahara, *Angew. Chem. Int. Ed.* **2016**, *55*, 3600–3605.
4. X. G. Meng, L. Q. Liu, S. Z. Ouyang, H. Xu, D. F. Wang, N. Q. Zhao, J. H. Ye, *Adv. Mater.* **2016**, *28*, 6781–6803.
5. W. L. Yang, L. Zhang, J. F. Xie, X. D. Zhang, Q. H. Liu, T. Yao, S. Q. Wei, Q. Zhang, Y. Xie, *Angew. Chem. Int. Ed.* **2016**, *55*, 6715–6719.
6. X. Y. Ma, J. Q. Li, C. H. An, J. Feng, Y. H. Chi, J. X. Liu, J. Zhang, Y. G. Sun, *Nano Res.* **2016**, *9*, 2284–2293.
7. M. H. Sun, S. Z. Huang, L. H. Chen, Y. Li, X. Y. Yang, Z. Y. Yuan, B. L. Su, *Chem. Soc. Rev.* **2016**, *45*, 3479–3563.
8. Q. H. Liang, Z. Li, X. L. Yu, Z. H. Huang, F. Y. Kang, Q. H. Yang, *Adv. Mater.* **2015**, *27*, 4634–4639.
9. B. Yang, K. J. Edler, *Chem. Mater.* **2009**, 21, 1858–1866.
10. M. L. Cortez, M. Ceolín, O. Azzaroni, F. Battaglini, *Anal. Chem.* **2011**, *83*, 8011–8018.
11. S. Pullen, H. Fei, A. Orthaber, S. M. Cohen, S. Ott, *J. Am. Chem. Soc.* **2013**, *135*, 16997–17003.
12. A. Dhakshinamoorthy, A. M. Asiri, H. García, *Angew. Chem. Int. Ed.* **2016**, *55*, 5414–5445.
13. Y. B. Huang, J. Liang, X. S. Wang, R. Cao, *Chem. Soc. Rev.* **2017**, *46*, 126–157.
14. Y. Li, H. Xu, S. Ouyang, J. Ye, Phys. *Chem. Chem. Phys.* **2016**, *18*, 7563–7572.
15. X. J. Kong, Z. Lin, Z. M. Zhang, T. Zhang, W. Lin, *Angew. Chem. Int. Ed.* **2016**, *55*, 6411–6416.
16. J. D. Xiao, Q. C. Shang, Y. J. Xiong, Q. Zhang, Y. Luo, S. H. Yu, H. L. Jiang, *Angew. Chem. Int. Ed.* **2016**, *55*, 9389–9393.
17. G. K. H. Shimizu, R. Vaidhyanathan, J. M. Taylor, *Chem. Soc. Rev.* **2009**, *38*, 1430–1449.
18. T. Kimura, *Angew. Chem. Int. Ed.* **2017**, 56, 13459–13463.
19. Y. P. Zhu, T. Z. Ren, Z. Y. Yuan, *Catal. Sci. Technol.* **2015**, *5*, 4258–4279.
20. C. F. J. Faul, M. Antonietti, *Adv. Mater.* **2003**, 15, 673–683.
21. K. Kogej, *Adv. Colloid Interface Sci.* **2010**, *158*, 68–83.
22. C. Shi, W. Wang, N. Liu, X. Xu, D. Wang, M. Zhang, P. Sun, T. Chen, *Chem. Commun.* **2015**, *51*, 1345–1348.
23. J. G. Wang, H. J. Zhou, P. C. Sun, D. T. Ding, T. H. Chen, *Chem. Mater.* **2010**, *22*, 3829–3831.
24. X. N. Wei, X. Shi, *J. Phys. Chem. C* 2014, *118*, 4213–4221.
25. J. E. Haskouri, C. Guillem, J. Latorre, A. Beltrán, D. Beltrán, P. Amorós, Chem. Mater. 2004, 16, 4359–4372.
26. T. Kimura, *Chem. Mater.* 2005, *17*, 5521–5528.
27. Z. Xu, M. Quintanilla, F. Vetrone, A. O. Govorov, M. Chaker, D. Ma, *Adv. Funct. Mater.* **2015**, *25*, 2950–2960.
28. Y. P. Zhu, T. Y. Ma, T. Z. Ren, J. Li, G. H. Du, Z. Y. Yuan, *Appl. Catal. B: Environ.* **2014**, *156–157*, 44–52.
29. J. Sun, J. Zhang, M. Zhang, A. Antonietti, X. Fu, X. Wang, *Nat. Commun.* **2012**, *3*, 1139.
30. J. Liu, Y. Liu, N. Liu, Y. Han, X. Zhang, H. Huang, Y. Lifshitz, S. T. Lee, J. Zhong, Z. Kang, *Science* 2015, *347*, 970–974.
31. H. Yaghoubi, Z. Li, Y. Chen, H. T. Ngo, V. R. Bhethanabotla, B. Joseph, S. Ma, R. Schlaf, A. Takshi, *ACS Catal.* **2015**, *5*, 327–335.
32. J. Ran, T. Y. Ma, G. Gao, X. W. Du, S. Z. Qiao, *Energy Environ. Sci.* **2015**, *8*, 3708–3717.
33. G. Zhang, M. Zhang, X. Ye, X. Qiu, S. Lin, X. Wang, *Adv. Mater.* **2014**, *26*, 805–809.
34. G. Liu, L. Wang, C. Sun, X. Yan, X. Wang, Z. Chen, S. C. Smith, H. M. Cheng, G. Q. Lu, *Chem. Mater.* **2009**, *21*, 1266–1274.
35. L. Li, J. Yan, T. Wang, Z. J. Zhao, J. Zhang, J. Gong, N. Guan, *Nat. Commun.* **2014**, *6*, 5881.
36. Y. Liu, B. Zhang, L. Luo, X. Chen, Z. Wang, E. Wu, D. Su, W. Huang, *Angew. Chem. Int. Ed.* **2015**, *54*, 15260–15265.
37. N. D. Kim, D. B. Buchholz, G. Casillas, M. José-Yacaman, R. P. H. Chang, *Adv. Funct. Mater.* **2014**, 24, 4186–4194.
38. H. Li, H. Yu, X. Quan, S. Chen, H. Zhao, *Adv. Funct. Mater.* **2015**, *25*, 3074–3080.
39. J. Zhang, M. Zhang, C. Yang, X. Wang, *Adv. Mater.* **2014**, *26*, 4121–4126.
40. Q. Han, B. Wang, Y. Zhao, C. Hu, L. Qu, *Angew. Chem. Int. Ed.* **2015**, *54*, 11433–11437.

COMMUNICATION

COMMUNICATION

An interesting photocatalyst structure: A new metal-organic framework (MOF) nanostructure synthesized by a surfactant-directed strategy features a stable framework of titanium phosphates, well-defined sphere, and hierarchical nanopores, ensuring the competitive photoactivity in evolving hydrogen under both visible light and full-spectrum simulator irradiation, along with a high durability.
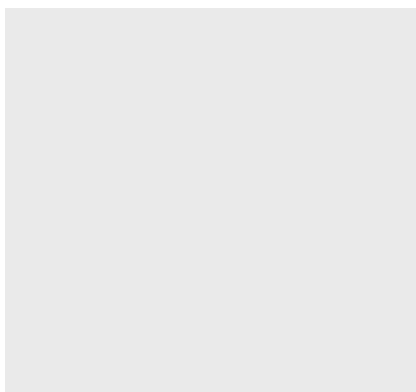
H. Li, Y. Sun, Z. Y. Yuan, Y. P. Zhu,* T. Y. Ma*

Page No. – Page No.

Titanium-Phosphonate-Based Metal-Organic Frameworks with Hierarchical Porosity for Enhanced Photocatalytic Hydrogen Evolution

Accepted Manuscript